Int. J. Electrochem. Sci., 17 **(2022)** Article Number: 220642, doi: 10.20964/2022.06.31

International Journal of ELECTROCHEMICAL SCIENCE
www.electrochemsci.org

Investigation on Effects of Avocado Extract as Eco-friendly Inhibitor for 201 Stainless Steel corrosion in Acidic Environment

A. F. Shoair[1,], Mai M. A. H. Shanab[2], M. H. H. Mahmoud[3], Z. I. Zaki[3], H. M. Abdel-Ghafar[4,5], M. M. Motawea[6,7]*

[1] Department of Science and Technology, University College - Ranyah, Taif University, Saudi Arabia.
[2] Department of Chemistry, College of Science & Humanity Studies, Prince Sattam Bin Abdulaziz University, P.O. Box: 13 Hawtat Bani Tamim 11149, Saudi Arabia & Forensic and Toxicology Lab., Forensic Medicine, Mansoura, Egypt.
[3] Department of Chemistry, College of Science, Taif University, P.O. Box 11099, Taif, 21944, Saudi Arabia
[4] Central Metallurgical Research and Development Institute (CMRDI), P.O. Box 87, Helwan, Cairo, Egypt.
[5] Center of Excellence for Water, The American University in Cairo, P.O. Box 74, New Cairo 11835, Egypt.
[6] Department of Chemistry, College of Science, University of Bisha, Bisha, Kingdom of Saudi Arabia
[7] Delta Higher Institute of Engineering & Technology Mansoura, Egypt
[*]E-mail: afshaair@tu.edu.sa

Received: 11 February 2022 / *Accepted:* 1 April 2022 / *Published:* 7 May 2022

The inhibitory effect of using avocado extract (AE) on the corrosion of stainless steel type 201 (201SS) in 1M hydrochloric acid has been studied. Chemical tests such as mass loss test (ML) and electrochemical such as electrochemical impedance spectroscopy (EIS) and potentiodynamic polarization (PP) were used in this investigation. The results of these approaches showed that as the concentration of AE extract increase, their adsorption on the 201SS surface increases, and therefore the corrosion process lower. The Langmiur isotherm was observed to represent the adsorption of this extract on the surface of 201-SS. The inhibitory efficiency percent (%IE) and activation energy (Ea) were calculated in the presence and absence of AE. The corrosion rate was calculated and revealed that AE has good inhibition effect on 201-SS alloy surface inspection methods such as SEM, AFM, and FT-IR have also been used. It was found that all of these used methods are in agreement with each other.

Keyword: 201SS, HCl, EIS, SEM, AFM, FT-IR

1. INTRODUCTION

The avocado, commonly used for culinary purposes and in the cosmetics industry has had, for thousands of years, great importance in the diet and in the culture of many countries [1]. Acid pickling, industrial acid cleaning, acid decaling, and oil well acidizing are just a few of the applications for acid solutions in industry. “Hydrochloric acid, sulphuric acid, nitric acid, and other acids are widely utilized. Because acids are aggressive, inhibitors are commonly used to reduce the corrosive effects on metals. A corrosion inhibitor is a chemical that efficiently reduces the rate of corrosion of a metal exposed to that environment when applied to it in a little dose. The majority of studies [2] employ plant extract to decrease metal corrosion in different acidic solution. Corrosion can be prevented by applying a coating to metal surfaces, using cathodic protection, or adding corrosion inhibitors. Corrosion inhibitors have been widely used and have proven to be highly effective in controlling the corrosion process [3]. An important measure for using an inhibitor in a large-scale industry is that it can be broken down by microorganisms, that it is non-toxic, and that it is not a pollutant, making it safe for the environment and human health” [4]. Researchers are currently working on additional natural corrosion inhibitors that are safe for the environment, non-toxic, and readily available. Natural chemical sources are rich in plant extracts. Simple processes may be used to extract it, and it is inexpensive and easily decomposes in nature [5].

It is well known that most of the extract containing heteroatoms, such as oxygen, nitrogen, sulfur, and phosphorus atoms easily form a layer of extract-iron complexes by absorption on steel surfaces and result in corrosion protection in acidic solution and a protective stop of the cathodic as well as anodic reaction at the steel interface / acidic.

In this work, the effective constituents contributing to the inhibition performance of avocado extract were investigated, and its corrosion inhibitory mechanism was discussed based on the results of surface characterization using SEM, AFM, and FTIR.

2. EXPERIMENTAL MEASUREMENTS

2.1. Materials and solutions

The stainless steel type 201 utilised had a percentage composition of 0.08 percent C, 2% Mn, 0.045 percent P, 0.030 percent S, 18 percent Cr, 0.75 percent Si, 8% Ni, 0.10 percent N, and lastly 80 percent Fe. The steel was chopped into pieces that were of the same size: 20 x 20 x 2 mm. The coupons had holes drilled in them to allow for the insertion of a hanger, which made it easier to remove the coupons. Different grades of emery or abrasive paper were used to grind the coupons: 160, 220, 320, 600, 1000, and 1500 grits. The specimens were completely cleaned with acetone, dried, and stored for subsequent testing in a local desiccator. Dilute a reagent of analytical grade HCl 37 percent with bi-distilled water to make the acid corrosive medium.

2.2. Avocado extract Procedure

Avocado extracts containing phenolic and flavonoids, as well as “triterpenoids, quinones, saponins, tannins, monoterpenoids, and sesquiterpenoids, even a tannin content of 13.6 percent tannins and 13.25 percent starch [6]. 500 g avocado dry powder was extracted with ethanol in a three-day maceration process. Filtration is done on the macerated extract. The filtrate was collected, and the residue was re-extracted for three days with ethanol before being filtered again. A rotary evaporator is used to concentrate the filtrate, yielding the concentrated extract. To eliminate the solvent, the concentrated extract was air-dried. As a stock solution, use an avocado extract solution with a concentration of 1000 ppm". As test solutions, inhibitor solutions with varied concentrations of 5, 10, 15, 20, 25, and 30 ppm were produced from these stock solutions.

2.3. Mass loss measurements (ML):

We cut the 201SS metal into six pieces, each of them (20 x20 x 2 mm). Before conducting the experiment, we sand the pieces using sandpaper from coarse to fine grades from (200-2000). Then we wash the pieces using distilled water and dry them, then acetone and dry them.By the aid of glass hooks in order to the whole surface of 201SS samples is completely immersed and uniformly attacked by corrosive solution [7-9]. The first piece is placed in 1 M HCl. The other pieces are putted in acid concentration with various concentration of inhibitors (5 to 30 ppm). After sanding and drying the pieces are weighed. The experiment lasts three hours. This experiment is repeated at different temperatures from (25^{o}C to 45^{o}C). The rates of corrosion (CR) , (%IE) and (θ) were calculated from the next balance [10].

$$\%IE= [1-(\Delta W_{inh} /\Delta\ W_{free})]\ x100 = \theta\ x100 \quad (1)$$

$$C.R = \Delta W \setminus at \quad (2)$$

Since ΔW_{inh} and ΔW_{free} are the mass losses in inhibitor involvement and absence, respectively.

Where ΔW is the mass loss in mg, a is the area in cm^{-2}, t is the time in min.

2.4. Electrochemical techniques

2.4.2. PP tests

A three-compartment Pyrex glass cell was used for the PP method. The potential range was (-800 to +200 mV vs. SCE) at OCP with a scan rate of 0.2 mVs^{-1}. The i_{corr} calculation was utilized to measure the E_p and the θ from the following Eq. (3):

$$\%E_p= \theta\ x100= [1-(i_{corr}/i^{o}_{corr})]\ x\ 100 \quad (3)$$

Where i^{o}_{corr} and i_{corr} are corrosion current densities of uninhibited and inhibited solution, respectively.

2.4.3. EIS tests

AC signs with a peak-to-peak amplitude of 10 mV and a frequency range of 10^{5} Hz to 0.01Hz was used to measure EIS.

2.5. Surface morphology investigation by (SEM, AFM, and FT-IR) analysis

The applied technique to study metal surface morphology are SEM, AFM, and FT-IR it is used to give data about the surface morphology of 201SS coins with and without highest degree of concentration of the avocado inhibitor utilizing (SEM model JOEL, JSM-T20, Japan). Atomic force microscope (AFM) is an actual test using for examing the morphology of 201SS surface at nano- to micro- scale. The chemical characterization of the avocado extract was executed by Fourier Transform Infrared Spectroscopy (FTIR) using the Attenuated Total Reflectance (ATR) Thermo Scientific Nicolet, model IS10. The beam accelerating voltage was 25 kV.

3. RESULTS AND DISCUSSION

3.1. ML measurements

3.1.1. Effect of concentrations and temperature

The corrosion rate of 201SS metal was investigated in 1.0 M HCl at 25-45 °C in the absence and presence of various amounts of avocado inhibitor (5 to 30 ppm).

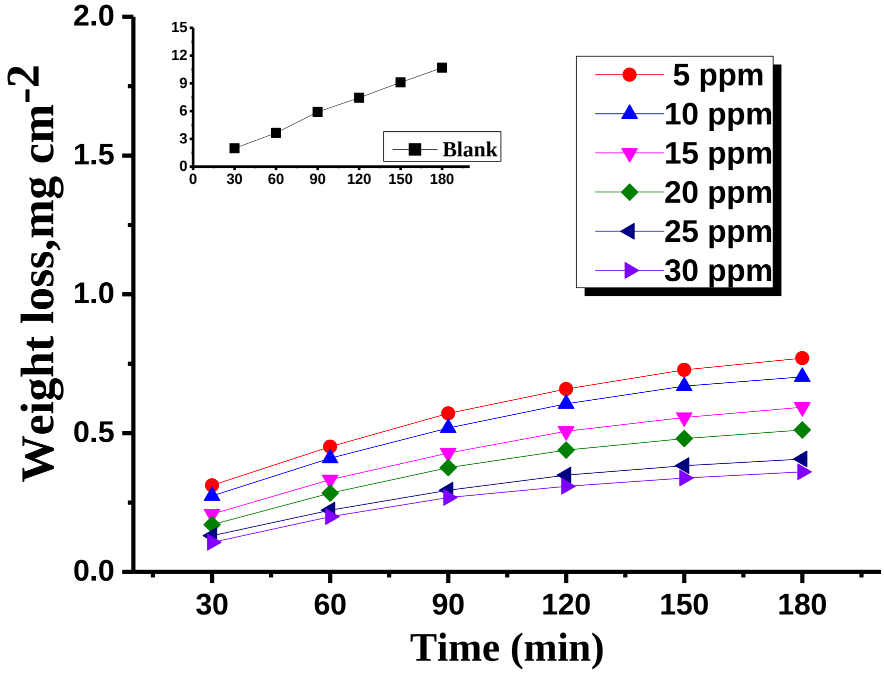

Figure 1. WL- time curves for dissolution of 201SS in 1M HCl with and without different concentration of avocado extract at 25°C.

Figure 1 depicts the WL-time curves graphically. Corrosion parameters derived from WL test at altered temperatures are given in Table 1, illustrate the designed values of k_{corr} ($mg.cm^{-2}.min^{-1}$), (%IE) and the (θ) for 201SS metal dissolution from which a reduction in k_{corr} is noticed when the concentration of avocado increases. This behavior can be explained based on the strong interaction among avocado and 201SS metal surface [11]**.** In general, when the concentration of extract rises, the value of (% IE) rises as well. These findings provide evidence that extract are effective inhibitors of 201SS metal dissolution. [12]. Temperature affects corrosion parameters, and while increased temperatures lead to decreased adsorption of inhibitor molecules on the surface of 201SS.

Table 1. Corrosion rate, Ɵ and %E of avocado at different temperatures.

Temp., ^{o}C	Conc, ppm	k_{corr} (mg cm^{-2} min^{-1})	Ɵ	%IE
25	Blank	0.0730	--	--
	5	0.0077	0.893	89.3
	10	0.0068	0.906	90.6
	15	0.0061	0.915	91.5
	20	0.0058	0.919	91.9
	25	0.0051	0.929	92.9
	30	0.0049	0.932	93.2
30	Blank	0.0880	--	--
	5	0.0111	0.874	87.4
	10	0.0097	0.890	89.0
	15	0.0091	0.897	89.7
	20	0.0089	0.899	89.9
	25	0.0087	0.901	90.1
	30	0.0082	0.907	90.7
35	Blank	0.1030	--	--
	5	0.0158	0.847	84.7
	10	0.0145	0.859	85.9
	15	0.0139	0.865	86.5
	20	0.0123	0.881	88.1
	25	0.0119	0.884	88.4
	30	0.0108	0.895	89.5
40	Blank	0.1350	---	---
	5	0.0330	0.756	75.6
	10	0.0280	0.793	79.3
	15	0.0195	0.856	85.6
	20	0.0182	0.865	86.5
	25	0.0171	0.873	87.3
	30	0.0161	0.881	88.1
45	Blank	0.1530	---	---
	5	0.0405	0.735	73.5
	10	0.0377	0.754	75.4
	15	0.0366	0.761	76.1
	20	0.0341	0.777	77.7
	25	0.0312	0.796	79.6
	30	0.0274	0.821	82.1

3.1.2 Thermodynamic activation parameters

Corrosion reactions obey Arrhenius procedures and the apparent activation energy, E^*_a, for corrosion of 201SS metal in 1M HCl solution in the existence, and absence at altered dose of avocado extract at 25-45°C were calculated from Arrhenius Eq. [13]:

$$\log k_{corr} = \left(\frac{-E^*_a}{2.303RT}\right) + \log A \qquad (4)$$

Plots of log k_{corr} vs. 1/T are displayed as straight lines for the tested inhibitors and the E^*_a was measured from the slope of these lines Figure 2. It can be seen from Table 2 the data that E^*_a values for the inhibitors attains increase values for inhibitor-containing solutions signifies phsisorption.

Table 2. Activation parameter for 201SS dissolution in 1.0 M HCl with and without avocado inhibitor

C_{inh}, ppm	E_a^*, kJ /mol	ΔH^*, kJ /mol	$-\Delta S^*$, J /mol.K
Blank	41.5	38.9	121.0
5	64.2	61.6	60.2
10	66.5	63.9	53.4
15	68.7	66.1	46.5
20	71.0	68.4	39.8
25	71.8	69.2	38.3
30	72.5	69.9	37.4

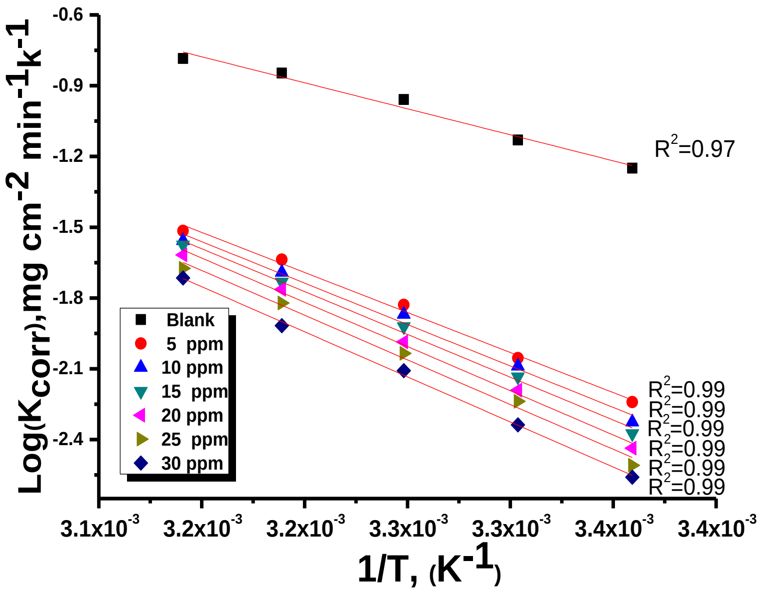

Figure 2. log K_{corr} vs. 1/T curves in the absence and presence of different concentrations of avocado extract for corrosion of 201SS in 1 M HCl.

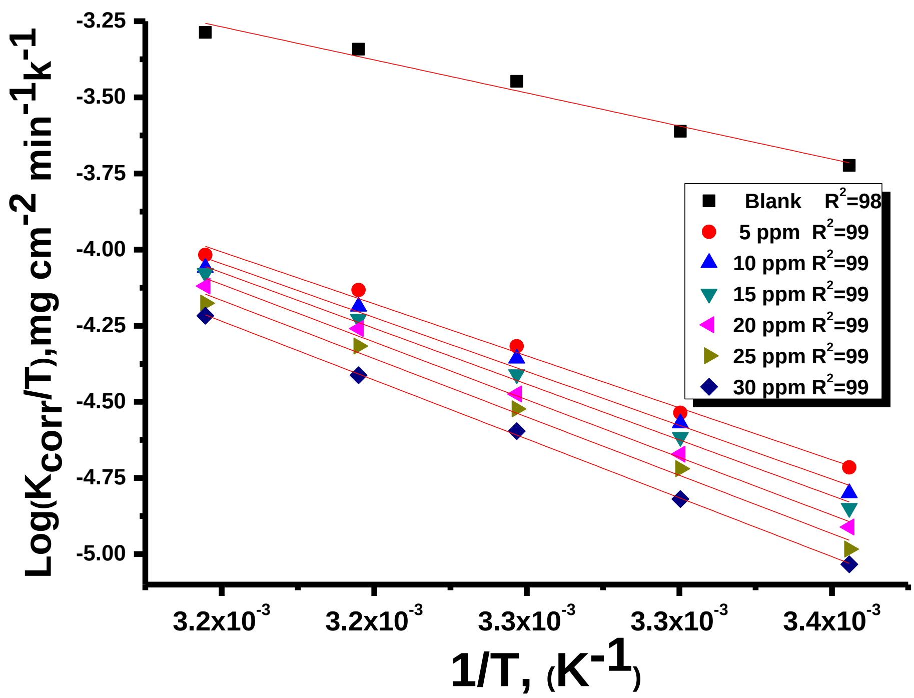

Figure 3. log (K_{corr} /T) vs. 1/T curves without and with of different concentrations of avocado extract for corrosion of 201SS in 1 M HCl.

The transition state equation was used to calculate other important thermodynamic activation parameters [14]:

$$\log k_{corr} = \log\left(\frac{R}{Nh}\right) + \frac{\Delta S^*}{2.303R} + \frac{\Delta H^*}{2.303RT} \qquad (5)$$

Where, “k_{corr} signifies to the corrosion rate, R is the gas constant, ΔH^* and ΔS^* is the enthalpy and entropy of activation, respectively. Plots of log k_{corr}/T vs. 1000/T in Figure 3, from which the values of ΔH^* and ΔS^*were calculated and are recorded in Table 2 for the investigated inhibitor”. Figure 2 shows $\boldsymbol{E_a^*}$ increased with increasing the concentrations of avocado inhibitors.

The increased value of $\boldsymbol{E_a^*}$ when AE inhibitors are existing is due to their adsorption on the 201SS surface. The phsisorption process [15] has this occurred. Positive ΔH^* values indicate that avocado molecules are adsorbed endothermically on the 201SS. The activation entropy ΔS^* is large and negative, indicating that the transition state includes association rather than dissociation in the creation of an activated complex, and that disorder decreases as reactants transform into the activated complex [16].

3.1.3 Adsorption study

It is clear that the adsorption of inhibitor on the metal surface obeys Langmuir isotherm. This adsorption isotherm is described by the following equation Eq. (6) [17]

$$\frac{C}{\theta} = \left(\frac{1}{K_{ads}}\right) + C \qquad (6)$$

A plot of (C/Θ) versus concentration of inhibitor gives straight lines. From intercept, the value of adsorption constant (K_{ads}) was calculated. By applying in the following equation, we calculate standard free energy of adsorption ($\Delta G°_{ads}$) was calculated from the next equation (7):

$$K_{ads} = \frac{1}{55.5} \exp\left(\frac{-\Delta G^{o}_{ads}}{R\,T}\right) \qquad (7)$$

Table 3 shows that the ΔG^{o}_{ads} achieved slightly more negative values than -20 kJ mol^{-1} and decrease with rising temperature, which accepts that the adsorbed layer is more stable at lower temperatures. This indicates that avocado inhibitors may adsorbed physically on 201SS surface [18]. Also, other important adsorption parameters were calculated such as the enthalpy (ΔH^{o}_{ads}) and the entropy (ΔS^{o}_{ads}) of adsorption by applying Van't Hoff and thermodynamic general equation (9) [19]:

$$\mathbf{ln K_{ads}} = \frac{-\Delta \mathbf{H^{o}}}{\mathbf{R\ T}} + \mathbf{constant} \qquad (8)$$

Figure 5 demonstrations draw among log K_{ads} and 1/T. From the slope of the line, ΔH^{o}_{ads} value can be measured. ΔS^{o}_{ads} can be obtained by applying the following Eq.

$$\mathbf{\Delta G^{o}_{ads} = \Delta H^{o}_{ads} - T\,\Delta S^{o}_{ads}} \qquad (9)$$

Table 3 reveals that positive values of ΔH^{o}_{ads} indicate that avocado extract adsorption is an exothermic process. Exothermic adsorption can be physical or chemical, but the value determines the kind of adsorption, suggesting that as the temperature rises, the inhibitory efficiency decreases. This manner can be explained by the fact that inhibitor molecules desorb to the 201-SS surface as the temperature rises [20]. Because the exothermic adsorption process is always accompanied by an increase in entropy, the value of ΔS^{o}_{ads} is negative in the presence of AE. An increase in entropy accelerated the adsorption of inhibitor onto the 201SS surface [21].

Table 3. Parameters obtained from avocado extract adsorbed on 201SS in 1M HCl acid at various temperatures.

T, K	K_{ads} M^{-1}	$-\Delta G°_{ads}$ kJ mol^{-1}	$\Delta H°_{ads}$ kJ mol^{-1}	$-\Delta S°_{ads}$ J mol^{-1} k^{-1}
298	257	23.7	38.0	79.0
303	158	22.8		75.1
308	104	22.1		71.0
313	84	21.9		70.3
318	51	21.0		66.0

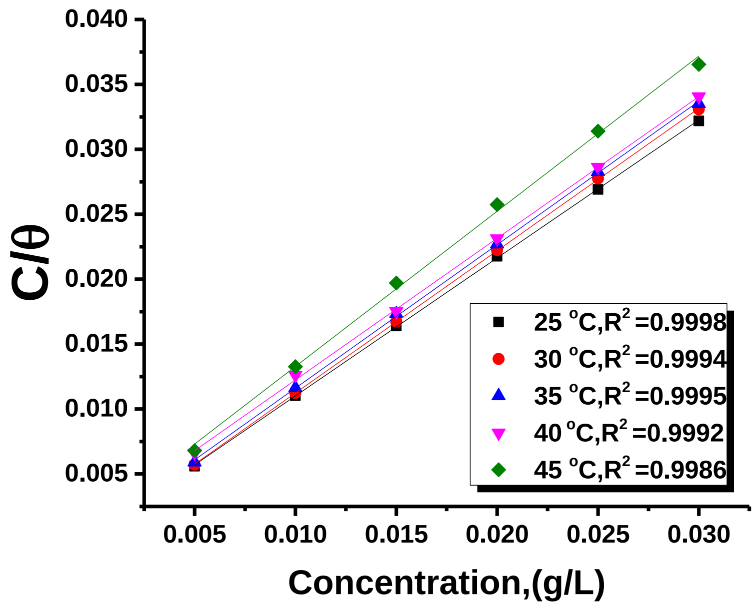

Figure 4. Langmuir curves for 201SS dissolution in the 1M HCl solution of avocado extract.

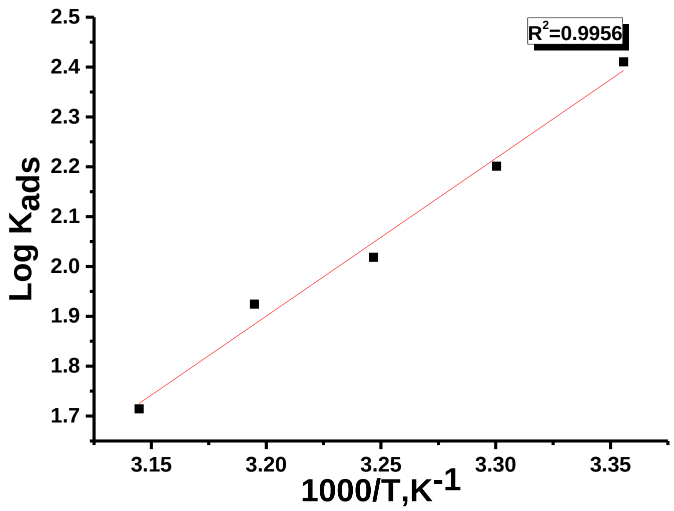

Figure 5. Log K_{ads} vs. 1/T curve for adsorption of avocado extract on the 201SS surface.

3.4. PP tests

Tafel polarization curves of 201SS metal in uninhibited and inhibited 1M HCl solution with various concentration of avocado extract at 25°C are illustrated in Figure 6**.** "The deviation of PP parameters with the concentration of avocado extract are given in Table 4. The PP indicates that, the behavior of avocado extract is of Tafel-type because the addition of extract increases the cathodic and anodic potential with a displacement to more negative and positive values, correspondingly. i_{corr} drops as the concentration of avocado increases, signifying that the presence of these compounds slows 201SS dissolution and that the degree of inhibition is proportional to the concentration. The maximum difference in E_{corr} values between the inhibited and uninhibited systems was less than 33 mV, indicating that the investigated avocado extract are mixed type inhibitors that affect both the cathodic and anodic polarization curves [22] . In other words, the slope of the cathodic or anodic polarization curves has little effect in the presence of avocado extract. This designates that there is no change of the mechanism of the process". The inhibitive action of avocado extract is initiated by adsorption on the reactive sites on the electrode surface and blocking corrosion cells and reducing the exposed surface area available for attack from corrosion environment.

Table 4. PP measurements for corrosion 201SS in 1M HCl with and without of various concentration of the avocado extract at 25°C.

[inh.] ppm	- $E_{corr,}$ mV(vs.SCE)	$i_{corr,}$ $\mu A\ cm^{-2}$	β_c $mV\ dec^{-1}$	β_a $mV\ dec^{-1}$	CR mpy	Θ	% IE
Blank	495	1540	122	66	594	----	----
5	489	572	126	72	352	0.629	62.9
10	484	427	121	56	195	0.723	72.3
15	480	330	113	57	150	0.786	78.6
20	475	215	115	60	107	0.860	86.0
25	471	125	120	62	61	0.919	91.9
30	462	104	111	54	55	0.932	93.2

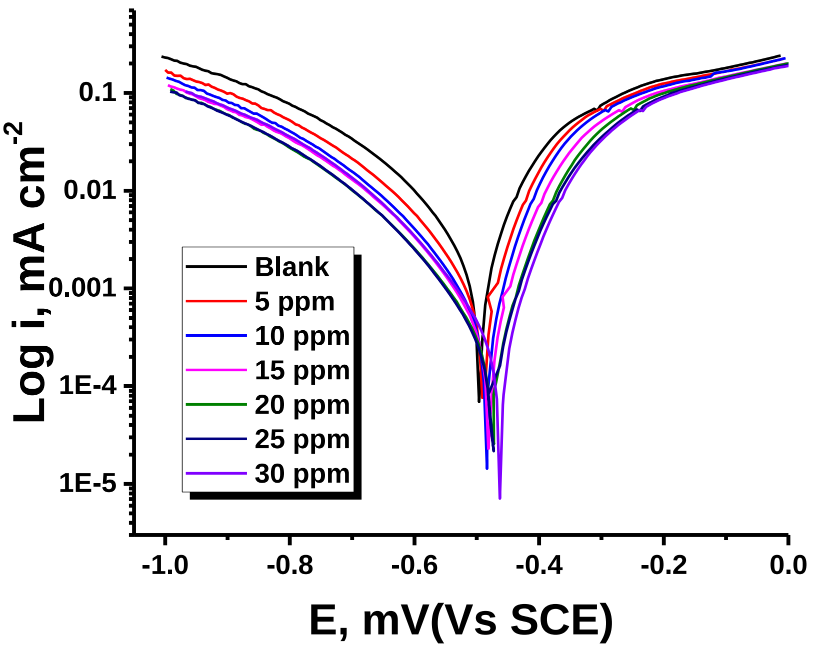

Figure 6. PP curves for dissolution 201SS in the 1M HCl solution at different concentration of avocado extract at 25°C.

3.5. EIS test

It showed Nyquist plots and Bode plots for 201SS dissolution in 1 M HCl in the attendance and non-existence of altered dose avocado extract at 25°C as represented in Figure 7,8. Charge–transfer resistance determines the impedance diagrams, which have a semi-circuit shape [23]. Surface roughness, contaminants, and inhibitor adsorption caused porous layers to form and the electrode surface to be homogeneous. Figure 9 shows how the obtained impedance data was analyses using the electrical equivalent circuit model. C_{dl} is defined as [24]:

$$C_{dl} = Y_o\,(\omega_{max})^{n-1} \qquad (10)$$

%IE and θ of the avocado extract obtained from impedance tests can be determined using the following relationships.

$$\%IE = [(R_{ct}-R^{o}_{ct})\backslash R_{ct}] \times 100 \qquad (11)$$

Where R^{o}_{ct} and R_{ct} charge transfer resistance of uninhibited and inhibited solution, respectively.

The diameter of Nyquist diagrams rises with improving the dose of avocado extract due to creation of adsorbed layer of the inhibitor on 201SS surface. From table 8, R_{ct} increase by increasing the dose of the avocado inhibitor due to corrosion rate decrease. C_{dl} values drop as avocado concentration rises, as adsorbed inhibitor molecules replace water molecules in the double layer to form an adherent film on the 201SS surface, lowering the dielectric constant at the metal-solution interface.

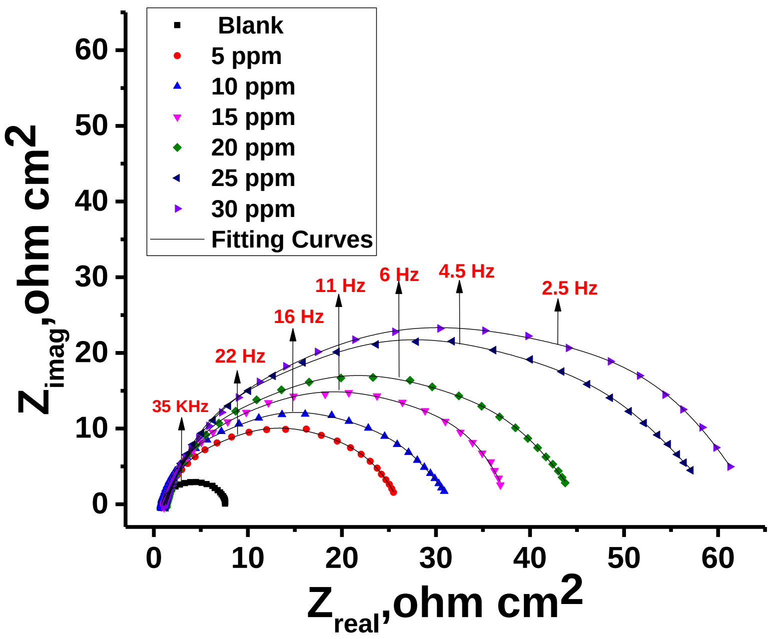

Figure 7. The Nyquist plot for dissolution of 201SS in 1 M HCl with and without different concentration of *Avocado inhibitor* at 25°C

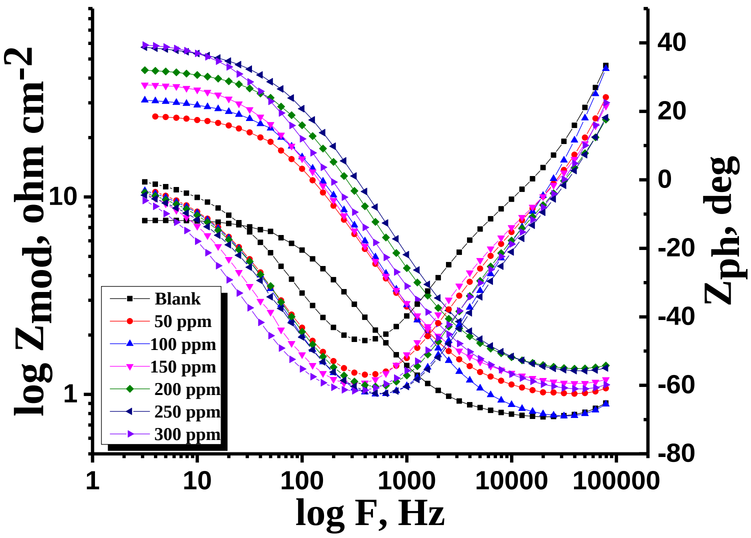

Figure 8. The Bode plot for dissolution of 201SS in 1 M HCl with and without different concentration of *Avocado inhibitor* at 25°C

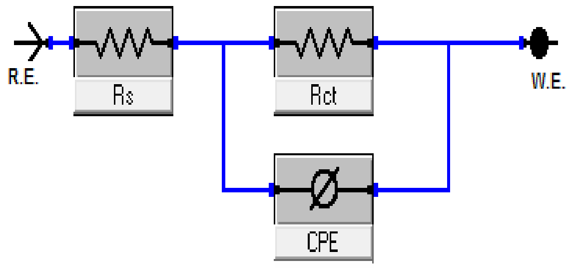

Figure 9. The circuit for appropriate the EIS data

Table 5. EIS for corrosion of 201SS with and without of altered doses of *avocado* extract at 25°C

Conc., ppm	Y_o, ($\mu\ \Omega^{-1}\ s^{n}\ cm^{-2}$) x$10^{-6}$	n	Rct, Ω cm2	Cdl, µF cm-2	Ө	% I.E
Blank	313	0.931	6	197	--	--
5	183	0.887	24	91	0.750	75.0
10	134	0.917	29	79	0.793	79.3
15	126	0.890	34	64	0.824	82.4
20	103	0.896	40	54	0.850	85.0
25	91	0.889	54	47	0.889	88.9
30	80	0.858	61	33	0.902	90.2

3.6. AFM Studies

The roughness of the 201SS morphology surface was determined using AFM experiments after dipping in 1 M HCl in attendance and a lack of 30 ppm of avocado extract for 24 h immersion. There is much less damage on the surface of 201SS with investigated avocado extract compared to blank in Figure 10 [25]. The mean roughness (Sa) of 201SS surface increased with immersion in 1 M HCl solution (Sa=643) and then decreased with adding investigated avocado to solution (Sa=103).

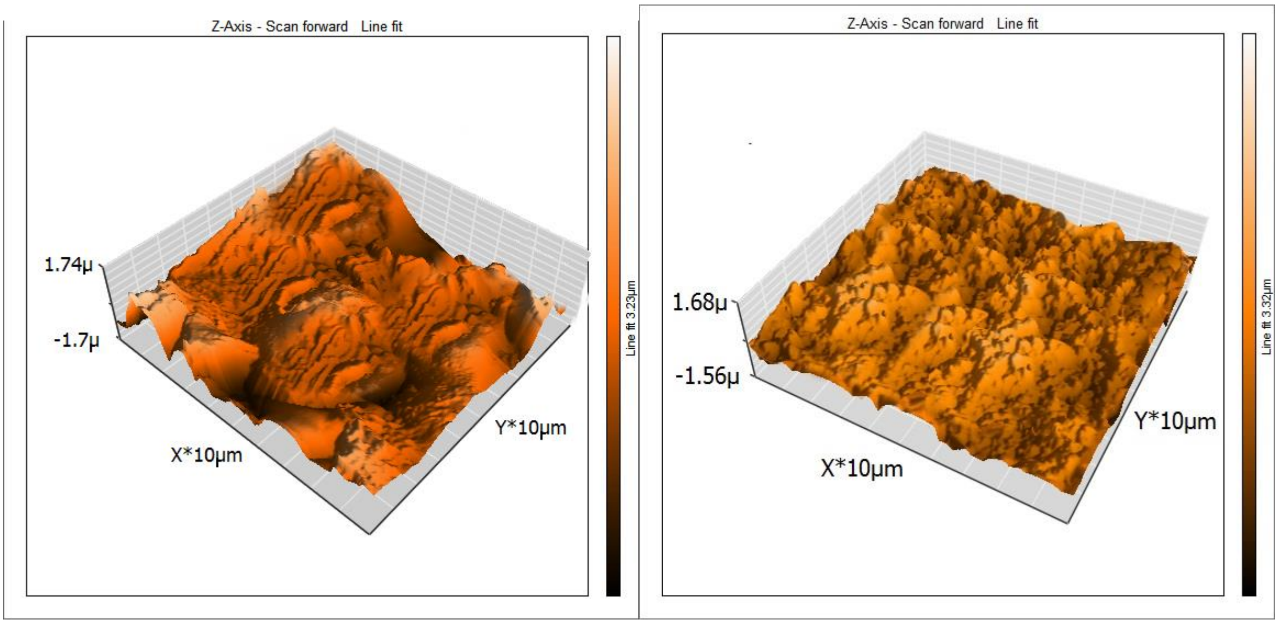

(a) (b)

Figure 10. AFM micrographs for 201SS in (a) Blank (b) inhibited solution of avocado extract

3.7. SEM studies:

The photograph of 201SS before immersion in acid solution shows the surface was smooth and without pits. The photograph of 201SS after immersion in acid solution shows the surface was strongly damaged. The photograph of 201SS after immersion in acid solution with the maximum concentration of the avocado inhibitor shows the surface was free from pits and it was smooth. In accordance, it was found that the adsorption film was formed on the 201SS surface and inhibit the corrosion of 201SS.

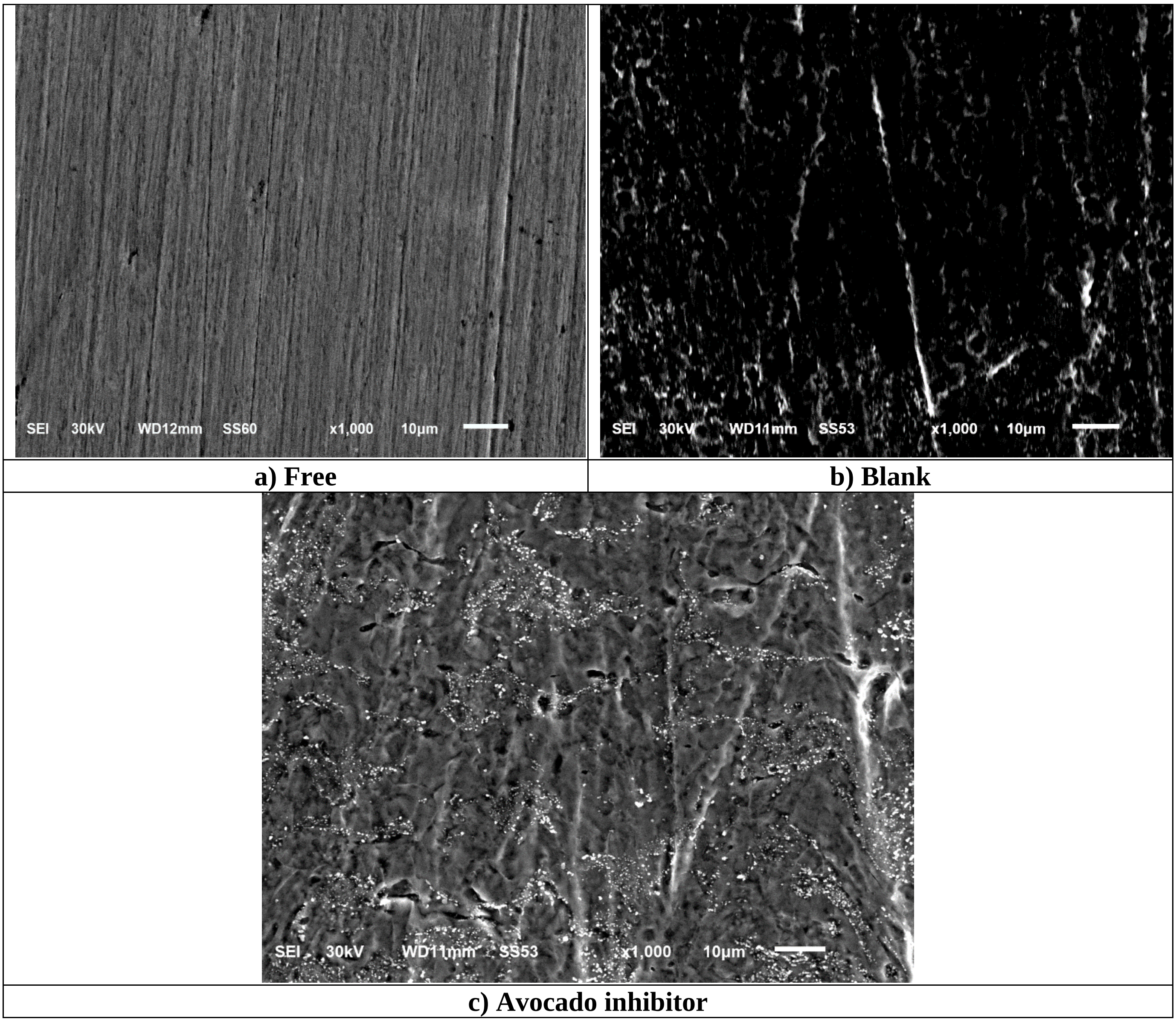

Figure 11. SEM micrographs for 201SS in (a) free sample (b) blank (c) inhibited solution of avocado extract.

3.8. FTIR technique

The IR spectra of appeared certain peaks which corresponded to the function groups in the extract. This Figure 12 showed that: The infrared spectrum, was obtained from the avocado powder. The peak centered at 3289 cm^{-1} can be attributed to O-H and also N-H groups, which can be found in water or amines. The peak at 2924 cm^{-1} can be associated to C-H stretching present in organic compounds. Around 1712 cm^{-1} is noticeable a band that can be associated to the carboxylate group (C=O), usually found in flavonoids and fatty acids. The band present in the 1150 cm^{-1} refers to aromatic rings, while the bands covered by the 1060-1080 cm^{-1} and 1010-1040 cm^{-1} ranges are referring to the stretching vibration of the C-O bond of alcohols and phenols. There is a slightly shift in the peaks of avocado inhibitor function groups which adsorbed on the 201SS surface and this indicate that avocado extract can act as corrosion inhibitors [26-27].

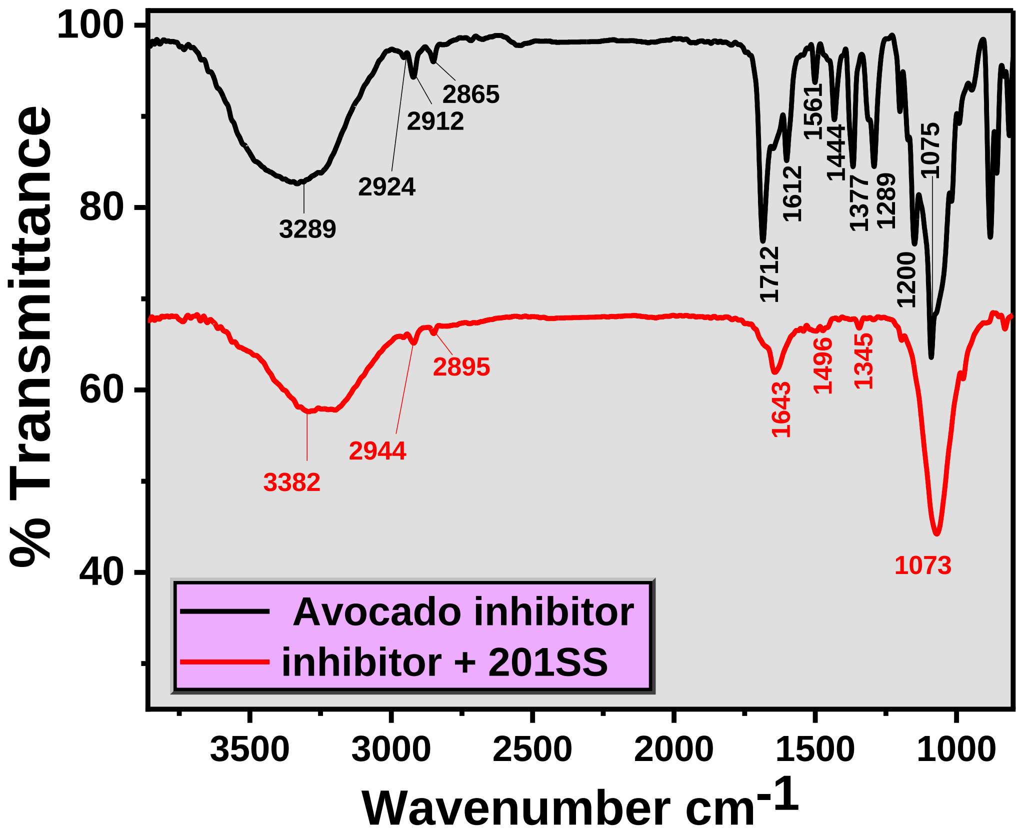

Figure 12. FT-IR spectrum of Avocado before and after adsorption on 201SS surface.

3.9. Mechanism of Corrosion Inhibition

The inhibition efficiency of *avocado* corrosion inhibitor against the corrosion of 201SS in 1 M HCl (via the physisorptions). “In the acid medium 201SS surface bear's positive charge, so it is testing to the protonated molecules to adsorb on the 201SS surface due to the electrostatic repulsion The avocado extract form adsorbed layer on the 201SS surface which block the active sites and decrease corrosion by prevention the attack of the surround corrosive medium” [28].The Cl^- ions get adsorbed on the positive charge (201SS surface) and turn it as negatively charged surface, the protonated inhibitor molecules (cationic) get adsorbed on the negatively charged surface of 201SS by an electrostatic attraction as shown below

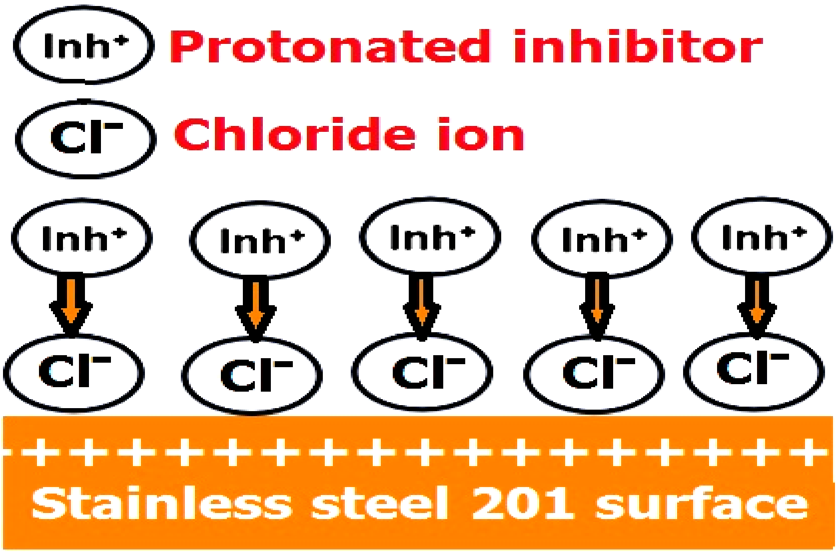

Table 6 show a variety of %IE of plant extracts have been reported as actual corrosion protection in acid solutions, particularly for steel. As can be seen in this Table the %IE of the present *avocado* extract is better than those of previously reported extracts.

Table 6. The following is a list of plant sources that were used in dissolution inhibition research.

Plant	Metal	Corrosive medium	%IE	Ref.
Punica granatum peel	(SS-410)	HCl	91	[29]
Tea tree extract	304 SS	1M HCl	83	[30]
Euphorbina heterophylla llinneo	MS	1.5M HCl	69	[31]
Ipomoea batatas	Galvanized steel	1M HCl	64.26	[32]
Cola acuminata extract	CS	1M HCl	74	[33]
Avocado extract	**201SS**	**1M HCl**	**93.2**	**This study**

4. CONCLUSION

The study revealed the investigated avocado were utilized as highly efficient inhibitors for 201SS in 1M HCl. "Results obtained from weight loss, polarization, EIS , AFM, FT-IR, and SEM techniques are in good agreement and show increased inhibitor efficiency with increasing inhibitor concentration. Adsorption of the inhibitor fits Langmuir isotherm model for 201SS. By raising the inhibitor dosage, the charge transfer resistance increases while the capacitance double layer drops, which may be attributed to inhibitor molecules adsorbed on the 201SS surface. Polarization data show that the investigated extract act as mixed-type inhibitor in 1M HCl". The surface examination confirms that the investigated compounds adsorbed on the metal.

ACKNOWLEDGEMENTS
The authors would like to thank Taif University Researchers Supporting Project number (TURSP-2020/158), Taif University, Taif, Saudi Arabia, for supporting this work

References

1. M. E. S. de Jesus, A. de Mendonça Santos, M. S. Tokumoto, F. Cotting, I. P. Aquino and V. R. Capelossi, *Brazilian J. Dev.*, 6 (2020) 77197.
2. A. S. Fouda, E. Abdel-Latif, H. M. Helal and A. El-Hossiany, *Russ. J. Electrochem.*, 57 (2021) 159.
3. S. Garai, S. Garai, P. Jaisankar, J. K. Singh and A. Elango, *Corros. Sci.*, 60 (2012) 193
4. N. A. Odewunmi, S. A. Umoren and Z. M. Gasem, *J. Environ. Chem. Eng.*, 3 (2015) 286.
5. M. Faustin, A. Maciuk, P. Salvin, C. Roos and M. Lebrini, *Corros. Sci.*, 92 (2015) 287.
6. A. S. Fouda, R. E. Ahmed and A. El-Hossiany, *Prot. Met. Phys. Chem. Surfaces*, 57 (2021) 398.
7. R. Haldhar, D. Prasad, I. Bahadur, O. Dagdag and A. Berisha, *J. Mol. Liq.*, 323 (2021) 114958..
8. A. S. Fouda, S. E. Badr, A. M. Ahmed and A. El-Hossiany, *Int. J. Corros. Scale Inhib.*, 10 (2021) 1011.
9. E. Peñaloza, C. Holandino, C. Scherr, P. I. P. de Araujo, R. M. Borges, K. Urech, S. Baumgartner and R. Garrett, *Molecules*, 25 (2020) 4006.
10. E. B. Agbaffa, E. O. Akintemi, E. A. Uduak and O. E. Oyeneyin, *Sci. Lett.*, 15 (2021) 23.
11. A. Ezzat, S. M. A. Motaal, A. S. Ahmed, H. B. Sallam, A. El-Hossiany and A. S. Fouda, *Biointerface Res. Appl. Chem.,* 12(5) (2022) 6415.
12. A. S. Fouda, S. A. Abd El-Maksoud, A. El-Hossiany and A. Ibrahim, *Int. J. Electrochem. Sci.*, 2019, 14 (2019) 2187.
13. A. S. Fouda, N. E. Al-Hazmi, H. H. El-Zehry and A. El-Hossainy, *J Appl Chem*, 9 (2020) 362.
14. N. Raghavendra, L. V Hublikar, S. M. Patil, P. J. Ganiger and A. S. Bhinge, *Bull. Mater. Sci.*, 42 (2019) 1.
15. O. A. Elgyar, A. M. Ouf, A. El-Hossiany and A. S. Fouda, *Biointerface Res. Appl. Chem.*, 11 (2021) 14344.
16. A. S. Fouda, S. A. Abd El-Maksoud, A. A. M. Belal, A. El-Hossiany and A. Ibrahium, *Int. J. Electrochem. Sci*, 13 (2018) 9826.
17. M. B. Ibrahim, Z. Sulaiman, B. Usman and M. A. Ibrahim, *World*, 4 (2019) 45.
18. A. S. Fouda, M. Abdel Azeem, S. A. Mohamed, A. El-Hossiany and E. El-Desouky, *Int. J. Electrochem. Sci.*, 14 (2019) 3932.
19. M. A. Ali, A. M. Ouf, A. El-Hossiany and A. S. Fouda, *Biointerface Res. Appl. Chem.*, 12(4) (2022) 5116.
20. S. Zhang, L. Hou, H. Du, H. Wei, B. Liu and Y. Wei, *Corros. Sci.*, 167 (2020) 108531.
21. A. S. Fouda, A. El-Mekabaty, I. E. I. Shaaban and A. El-Hossiany, *Prot. Met. Phys. Chem. Surfaces*, 57 (2021) 1060.
22. A. S. Fouda, M. Eissa and A. El-Hossiany, *Int. J. Electrochem. Sci.*, 13 (2018) 11096.
23. A. S. Fouda, S. Rashwan, A. El-Hossiany and F. E. El-Morsy, *J. Chem. Biol. Phys. Sci.*, 9 (2019) 1.
24. M. A. Khaled, M. A. Ismail, A. A. El-Hossiany and A. E.-A. S. Fouda, *RSC Adv.*, 11 (2021) 25314.
25. M. M. Motawea, A. El-Hossiany and A. S. Fouda, *Int. J. Electrochem. Sci*, 14 (2019) 1372.
26. N. Soltani, N. Tavakkoli, A. Attaran, B. Karimi and M. Khayatkashani, *Chem. Pap.*, 74 (2020) 1799.
27. A. S. Fouda, E.-S. El-Gharkawy, H. Ramadan and A. El-Hossiany, *Biointerface Res. Appl. Chem*, 11 (2021) 9786.
28. A. S. Fouda, S. A. Abd El-Maksoud, A. El-Hossiany and A. Ibrahim, *Int. J. Electrochem. Sci*, 14 (2019) 6045.
29. N. Bhardwaj, P. Sharma, L. Guo, O. Dagdag and V. Kumar, J. Mol. Liq., 346 (2022) 118237.
30. J.-Y. Kim, I. Shin and J.-W. Byeon, *Materials (Basel).*, 14 (2021) 5016.
31. O. A. Akinbulumo, O. J. Odejobi and E. L. Odekanle, *Results Mater.*, 5 (2020) 100074.
32. C. K. Anyiam, O. Ogbobe, E. E. Oguzie, I. C. Madufor, S. C. Nwanonenyi, G. C. Onuegbu, H.

C. Obasi and M. A. Chidiebere, *SN Appl. Sci.*, 2 (2020) 1.
33. A.-R. I. Mohammed, M. M. Solomon, K. Haruna, S. A. Umoren and T. A. Saleh, *Environ. Sci. Pollut. Res.*, 27 (2020) 34270.